Appendix A

A.1 Interference Visibility

In Fig. 2.19 we have illustrated the measurement of the longitudinal coherence length with a Michelson interferometer showing a curve of the intensity of the interfering waves versus the path difference $2\Delta L$. The degree of modulation of this curve decreases with increasing path difference. If the path difference is large compared to the coherence length L_c, then this modulation vanishes. In the following we present a more precise description of interference visibility related to the spectral width of the light source. This interference visibility or *contrast of interference* is defined as follows:

$$C = \left| \frac{I_{max} - I_{min}}{I_{max} + I_{min}} \right|, \tag{A.1.1}$$

where I_{max} and I_{min} are the maximum and minimum intensities of the superimposed waves. For $I_{min} = 0$ the contrast achieves its maximum value $C = 1$. In general the interference of two waves leads to the resulting intensity described by (cf. 7.18):

$$I = I_1 + I_2 + 2\sqrt{I_1 I_2}\cos\delta, \tag{A.1.2}$$

with I_1, I_2 intensity of the single waves and δ the phase difference between the two waves at the point of interference. The phase difference is described by:

$$\delta = k(s_1 - s_2) + \delta_1 - \delta_2, \tag{A.1.3}$$

where k is the angular wave number for each wave, s_1 and s_2 the pathes travelled by wave 1 and wave 2; δ_1, δ_2 the initial phases of the waves at the chosen origin. In the case of monochromatic waves of the same angular wave number—as assumed so far—we obtain from (A.1.1) and (A.1.2):

$$C = \frac{2\sqrt{I_1 I_2}}{I_1 + I_2}. \tag{A.1.4}$$

A. Donges and R. Noll, *Laser Measurement Technology*, Springer Series in Optical Sciences 188, DOI: 10.1007/978-3-662-43634-9,

For simplicity, we consider the case, where the superimposed waves have the same intensity, i.e.:

$$I_0 = I_1 = I_2. \tag{A.1.5}$$

For two monochromatic waves follows then from (A.1.4) and (A.1.5), that the contrast of interference is $C = 1$. With (A.1.5) inserted in (A.1.2) we have:

$$I = 2I_0(1 + \cos\delta). \tag{A.1.6}$$

Let us now extend our considerations by assuming a light source which emits—instead of a single angular wave number, i.e. a pure monochromatic wave—a spectrum of waves. We describe the spectral intensity I_k of this light source by the following function:

$$I_k = \frac{\mathrm{d}I}{\mathrm{d}k} = f(k), \tag{A.1.7}$$

with k angular wave number. We can generalize (A.1.6) with the help of (A.1.7):

$$I = 2\int_{-\infty}^{\infty} f(k)(1 + \cos(\delta))\ \mathrm{d}k. \tag{A.1.8}$$

We assume that the function $f(k)$ describing the spectrum of the light source is symmetric with respect to an angular wave number k_0. Introducing new variables and definitions:

$$k' = k - k_0, \tag{A.1.9}$$

$$f(k) = f(k' + k_0) = f^*(k') \tag{A.1.10}$$

allows to rewrite (A.1.8) with (A.1.3):

$$I = 2\int_{-\infty}^{\infty} f^*(k')\ \mathrm{d}k' + 2\int_{-\infty}^{\infty} f^*(k')\cos[(k' + k_0)(s_1 - s_2) + \delta_1 - \delta_2]\ \mathrm{d}k'. \tag{A.1.11}$$

With the abbreviations $\Delta s = s_1 - s_2$ and $\Delta\delta = \delta_1 - \delta_2$ and Euler's formula the second integral in (A.1.11) is rewritten:

$$\int_{-\infty}^{\infty} f^*(k')\frac{\mathrm{e}^{\mathrm{i}[(k'+k_0)\Delta s+\Delta\delta]} + \mathrm{e}^{-\mathrm{i}[(k'+k_0)\Delta s+\Delta\delta]}}{2}\ \mathrm{d}k'$$

$$= \frac{1}{2}\int_{-\infty}^{\infty} \left[f^*(k')\mathrm{e}^{\mathrm{i}k'\Delta s\mathrm{i}(k_0\Delta s+\Delta\delta)} + f^*(k')\mathrm{e}^{-\mathrm{i}k'\Delta s}\mathrm{e}^{-\mathrm{i}(k_0\Delta s+\Delta\delta)}\right]\ \mathrm{d}k'. \tag{A.1.12}$$

With the substitution $\tilde{k} = -k'$ follows:

$$\int_{-\infty}^{\infty} f^*(k')\mathrm{e}^{-\mathrm{i}k'\Delta s}\mathrm{d}k' = \int_{\infty}^{-\infty} f^*(-\tilde{k})\mathrm{e}^{\mathrm{i}\tilde{k}\Delta s}(-\mathrm{d}\tilde{k}) = \int_{-\infty}^{\infty} f^*(\tilde{k})\mathrm{e}^{\mathrm{i}\tilde{k}\Delta s}\mathrm{d}\tilde{k}. \quad \text{(A.1.13)}$$

With (A.1.13) we have for (A.1.12):

$$\frac{1}{2}\int_{-\infty}^{\infty} f^*(k')\mathrm{e}^{\mathrm{i}k'\Delta s}2\cos(k_0\Delta s + \Delta\delta)\ \mathrm{d}k'. \quad \text{(A.1.14)}$$

Inserting (A.1.14) into relation (A.1.11) for the second integral then yields:

$$I = 2\left[\int_{-\infty}^{\infty} f^*(k')\ \mathrm{d}k' + \cos(k_0\Delta s + \Delta\delta)\int_{-\infty}^{\infty} f^*(k')\mathrm{e}^{\mathrm{i}k'\Delta s}\mathrm{d}k'\right]. \quad \text{(A.1.15)}$$

Finally, the interference contrast is with (A.1.15) and (A.1.1):

$$C(\Delta s) = \left|\frac{\int_{-\infty}^{\infty} f^*(k')\mathrm{e}^{\mathrm{i}k'\Delta s}\mathrm{d}k'}{\int_{-\infty}^{\infty} f^*(k')\mathrm{d}k'}\right|. \quad \text{(A.1.16)}$$

The result (A.1.16) shows that the interference contrast as a function of the path difference Δs is proportional to the Fourier transform of the spectrum of the emitted light of the source.

To demonstrate (A.1.16) we consider the following two spectra of a light source:

$$f_1(k) = \frac{I_0\mathrm{e}^{-\frac{(k-k_0)^2}{2\sigma^2}}}{\sqrt{2\pi}\sigma}, \quad \text{(A.1.17)}$$

$$f_2(k) = \frac{I_0}{2\sqrt{2\pi}\sigma}\left[\mathrm{e}^{-\frac{(k-k_1)^2}{2\sigma^2}} + \mathrm{e}^{-\frac{(k-k_2)^2}{2\sigma^2}}\right], \quad \text{(A.1.18)}$$

where σ determines the width of the Gaussian function, k_0 angular wave number at which the function (A.1.17) attains a maximum; k_1, k_2 angular wave numbers at which the function (A.1.18) attains local maxima, I_0 total intensity of both sources. The functions $f_1(k)$ and $f_2(k)$ are defined in such a way, that

$$\int_{-\infty}^{\infty} f_j(k)\mathrm{d}k = I_0,\ j = 1,\ 2 \quad \text{(A.1.19)}$$

holds. Spectrum (A.1.17) describes e.g. a single mode laser source, whereas (A.1.18) is a simple representation of a laser running at two axial modes. The full width at half maximum of the function $f_1(k)$ is given by:

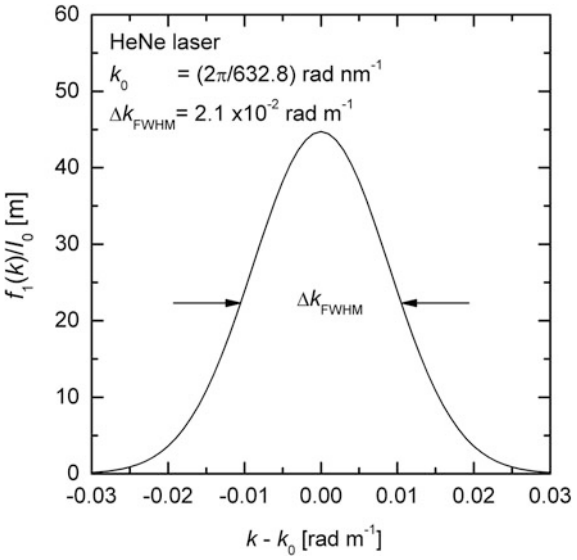

Fig. A.1 Spectrum of a HeNe laser as a function of the angular wave number difference $k - k_0$

$$\Delta k_{\mathrm{FWHM}} = 2\sqrt{2\ln 2}\sigma. \tag{A.1.20a}$$

Figure A.1 shows an example of the function $f_1(k)/I_0$.

(a) Contrast function (A.1.17):

Inserting (A.1.17) into (A.1.16) yields for the contrast function:

$$C_1(\Delta s) = \mathrm{e}^{-\Delta s^2\sigma^2/2}. \tag{A.1.20b}$$

Figure A.2 shows this contrast function. The key point is that the quantity σ appears in the denominator of the exponent of the spectrum (A.1.17) whereas in the contrast function σ occurs in the numerator of the exponent. From this follows that a broader spectrum, i.e. greater values of σ, lead to a contrast function decreasing faster with increasing Δs. The behaviour of the two functions—spectrum and contrast—is inverted. The broader the first one becomes, the narrower is the second, and vice versa. We have discussed already a similar feature while introducing the temporal coherence, see Sect. 2.4.2, where the coherence time is increasing, if the spectrum of a light source becomes narrower.

Let us now take the relations (2.28) and (2.29) from Chap. 2 describing the dependence of the coherence length L_c and the angular frequency width of the light source $\Delta\omega$:

$$\Delta\omega \frac{L_c}{c} = \pi. \tag{A.1.21}$$

We assume that $\Delta\omega$ refers to the full width of the spectrum of the light source at half maximum. With $\omega = kc$ and the differential thereof, we can rewrite (A.1.21):

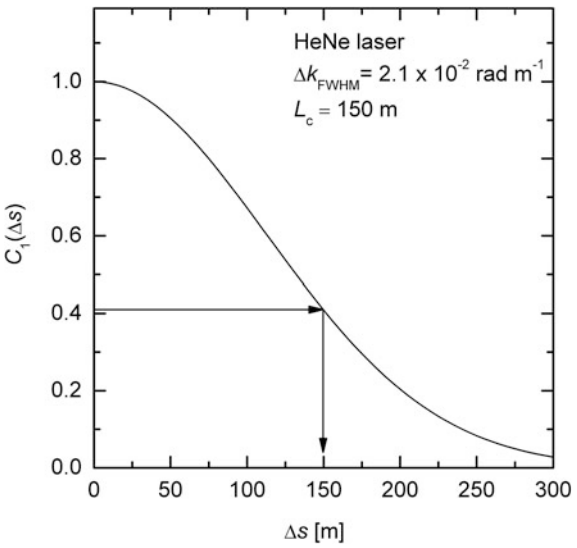

Fig. A.2 Contrast function belonging to the spectrum shown in Fig. A.1

$$\Delta k_{\mathrm{FWHM}} L_{\mathrm{c}} = \pi. \tag{A.1.22}$$

With (A.1.20a) and (A.1.20b) we can calculate the contrast if the path difference Δs is chosen to be just equal to the coherence length L_{c}:

$$C_1(\Delta s = L_{\mathrm{c}}) = \mathrm{e}^{-\frac{L_{\mathrm{c}}^2\sigma^2}{2}} = \mathrm{e}^{-\frac{\pi^2}{16\ln 2}} \approx 0.41. \tag{A.1.23}$$

The coherence length defined with relation (A.1.22) corresponds to a decrease of the contrast to about 0.41. This is a way to measure the coherence length by successively increasing the path difference Δs caused by the two interferometer arms of different lengths until the contrast function reaches the limit given in (A.1.23), then we have $L_{\mathrm{c}} = \Delta s$. For the chosen example, Fig. A.2 indicates the resulting coherence length of about 150 m. For a laser with this coherence length the frequency full width at half maximum is calculated with (A.1.21) and $\Delta\omega = 2\pi\Delta f$: $\Delta f = 1$ MHz. This frequency width divided by the frequency at the maximum of the spectrum amounts to 2.1×10^{-9}. This illustrates the extremely high spectral resolution achievable with a Michelson interferometer.

Instead of taking the right-hand side of (A.1.21) equal to π another value could be chosen, so that e.g. the contrast function yields 0.5 for $\Delta s = L_{\mathrm{c}}$:

$$\Delta\omega \frac{L_{\mathrm{c}}}{c} = 4\ln 2. \tag{A.1.24}$$

This is just a question of definition. With the analogous calculation steps as above, we find with (A.1.20b) and (A.1.24):

$$C_1(\Delta s = L_{\mathrm{c}}) = \mathrm{e}^{-\frac{L_{\mathrm{c}}^2\sigma^2}{2}} = \mathrm{e}^{-\frac{8(\ln 2)^2\sigma^2}{\Delta k_{\mathrm{FWHM}}^2}} = \mathrm{e}^{-\ln 2} = 0.5. \tag{A.1.25}$$

For the chosen example of Fig. A.1 and the right-hand side of (A.1.24) we obtain for the coherence length $L_c = 132$ m.

(b) Contrast function (A.1.18):

The contrast function (A.1.16) for the spectrum (A.1.18) is calculated with (A.1.9), (A.1.10) as follows:

$$C_2(\Delta s) = \frac{1}{2\sqrt{2\pi}\sigma}\left|\int_{-\infty}^{\infty} \mathrm{e}^{-\frac{(k'+k_0-k_1)^2}{2\sigma^2}}\mathrm{e}^{\mathrm{i}k'\Delta s}\mathrm{d}k' + \int_{-\infty}^{\infty} \mathrm{e}^{-\frac{(k'+k_0-k_2)^2}{2\sigma^2}}\mathrm{e}^{\mathrm{i}k'\Delta s}\mathrm{d}k'\right|. \quad \text{(A.1.26)}$$

The first integral can be solved with the help of the substitution $\tilde{k} = k' + k_0 - k_1$:

$$\int_{-\infty}^{\infty} \mathrm{e}^{-\frac{(k'+k_0-k_1)^2}{2\sigma^2}}\mathrm{e}^{\mathrm{i}k'\Delta s}\mathrm{d}k' = \mathrm{e}^{-\mathrm{i}(k_0-k_1)\Delta s}\int_{-\infty}^{\infty} \mathrm{e}^{-\frac{\tilde{k}^2}{2\sigma^2}}\mathrm{e}^{\mathrm{i}\tilde{k}\Delta s}\mathrm{d}\tilde{k} = \mathrm{e}^{-\mathrm{i}(k_0-k_1)\Delta s}\sqrt{2\pi}\sigma\,\mathrm{e}^{-\frac{\Delta s^2\sigma^2}{2}}. \quad \text{(A.1.27)}$$

In an analogous way we have for the second integral of (A.1.26):

$$\int_{-\infty}^{\infty} \mathrm{e}^{-\frac{(k'+k_0-k_2)^2}{2\sigma^2}}\mathrm{e}^{\mathrm{i}k'\Delta s}\mathrm{d}k' = \mathrm{e}^{-\mathrm{i}(k_0-k_2)\Delta s}\sqrt{2\pi}\sigma\,\mathrm{e}^{-\frac{\Delta s^2\sigma^2}{2}}. \quad \text{(A.1.28)}$$

Inserting (A.1.27) and (A.1.28) into (A.1.26) then yields:

$$\begin{aligned} C_2(\Delta s) &= \frac{1}{2}\mathrm{e}^{-\frac{\Delta s^2\sigma^2}{2}}\left|\mathrm{e}^{-\mathrm{i}(k_0-k_1)\Delta s} + \mathrm{e}^{-\mathrm{i}(k_0-k_2)\Delta s}\right| \\ &= \frac{1}{2}\mathrm{e}^{-\frac{\Delta s^2\sigma^2}{2}}\left|\mathrm{e}^{-\mathrm{i}k_0\Delta s}\right|\sqrt{(\mathrm{e}^{\mathrm{i}k_1\Delta s} + \mathrm{e}^{\mathrm{i}k_2\Delta s})(\mathrm{e}^{-\mathrm{i}k_1\Delta s} + \mathrm{e}^{-\mathrm{i}k_2\Delta s})}\ \ldots \\ &= \frac{1}{2}\mathrm{e}^{-\frac{\Delta s^2\sigma^2}{2}}\sqrt{2(1+\cos((k_2-k_1)\Delta s))} = \frac{1}{2}\mathrm{e}^{-\frac{\Delta s^2\sigma^2}{2}}\sqrt{2\cdot 2\cos^2\left(\frac{(k_2-k_1)}{2}\Delta s\right)}. \end{aligned} \quad \text{(A.1.29)}$$

So we have finally for the contrast function belonging to (A.1.18):

$$C_2(\Delta s) = \mathrm{e}^{-\frac{\Delta s^2\sigma^2}{2}}\left|\cos\left(\frac{(k_2-k_1)}{2}\Delta s\right)\right|. \quad \text{(A.1.30)}$$

Let us consider a HeNe laser with a resonator length of L_r, then the frequency spacing between two neighboring longitudinal modes of this laser is given by:

$$\Delta\nu = \frac{c}{2L_r}, \quad \text{(A.1.31)}$$

with c speed of light and L_r distance between the two resonator mirrors, cf. Sect. 2.5. As numerical example we take $L_r = 30$ cm and with (A.1.31) we obtain

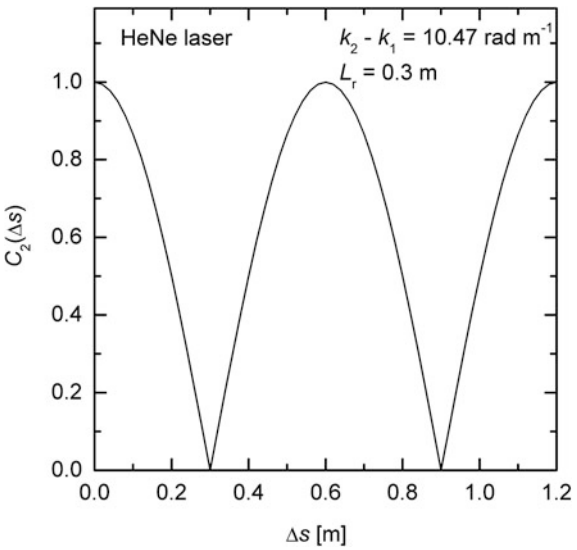

Fig. A.3 Contrast function belonging to the spectrum (A.1.18) of two neighboring axial modes of a HeNe laser

$\Delta\nu = 5 \cdot 10^8$Hz. The distance of the two longitudinal modes expressed with the angular wave numbers according to the definition chosen in (A.1.18) is then:

$$k_2 - k_1 = \frac{2\pi}{c}\Delta\nu = 10.47 \text{ rad m}^{-1}. \tag{A.1.32}$$

The resulting contrast function according to (A.1.30) is shown in Fig. A.3. The contrast varies periodically, a series of minima occur at odd integer multiples of the resonator length L_r. Starting with $\Delta s = 0$ and stepwise increasing Δs the first drop to $C_2(\Delta s) = 0.5$ appears for the following path difference:

$$\Delta s_{0.5} = \frac{2\pi}{3(k_2 - k_1)}. \tag{A.1.33}$$

A.2 Comparison of Spectral Radiance of the Emission of a Black Body and a Laser Source

The idea of this appendix is to provide the reader a numerical example of the significant differences of the spectral radiance emitted of a black body at thermal equilibrium and a laser source. The spectral radiance L_λ describes the emitted radiant flux divided by the unit area, the unit solid angle and the unit wavelength interval. Therefore, the unit of L_λ is W/(m^2 sr m). The spectral radiance of a black body is described by Planck's law [2]:

$$L_\lambda = \frac{2hc^2}{\lambda^5}\frac{1}{e^{hc/\lambda kT} - 1}, \tag{A.2.1}$$

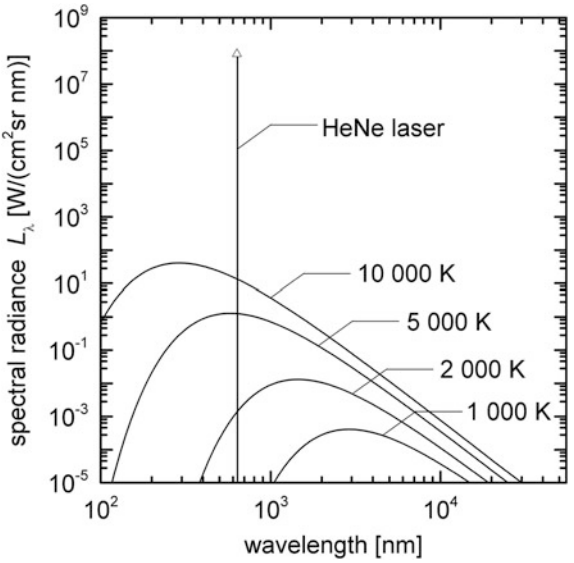

Fig. A.4 Spectral radiance of the radiation of a black body described by Planck's law for temperatures up to 10,000 K and spectral radiance of a HeNe laser with a flux of 1 mW, see text

with h Planck constant, c speed of light, λ wavelength, k Boltzmann constant and T temperature. Figure A.4 shows the spectral radiance of a black body for temperatures ranging from 1,000 to 10,000 K.

For comparison with a laser source we consider a HeNe laser emitting at $\lambda = 633$ nm taking the following exemplary data: flux $\phi = 1$ mW, full divergence angle $\Theta = 1$ mrad, beam diameter $d = 1$ mm, spectral line width $\Delta v = 1.5$ GHz. The latter can be transformed to a corresponding wavelength width with the help of the relation $c = \lambda v$:

$$|\Delta\lambda| = \frac{\lambda^2}{c}|\Delta v|. \tag{A.2.2}$$

Relation (A.2.2) yields then $\Delta\lambda = 2$ pm. The solid angle of the laser beam in the far field for a given divergence angle Θ is described by:

$$\Delta\Omega = 2\pi(1 - \cos(\Theta/2)). \tag{A.2.3}$$

This relation follows from the integral:

$$\Delta\Omega = \int_0^{2\pi} \int_0^{\Theta/2} \sin\theta \, \mathrm{d}\theta \, \mathrm{d}\varphi, \tag{A.2.4}$$

where φ is the azimuth angle, θ the polar angle. We can check whether (A.2.3) is plausible by inserting $\Theta = 2\pi$ in (A.2.3) which yields $\Delta\Omega = 4\pi$ sr, i.e. the full solid angle of a sphere.

With the given divergence angle of the laser beam we obtain $\Delta\Omega = 7.85 \times 10^{-7}$sr. The spectral radiance of the laser source is given by:

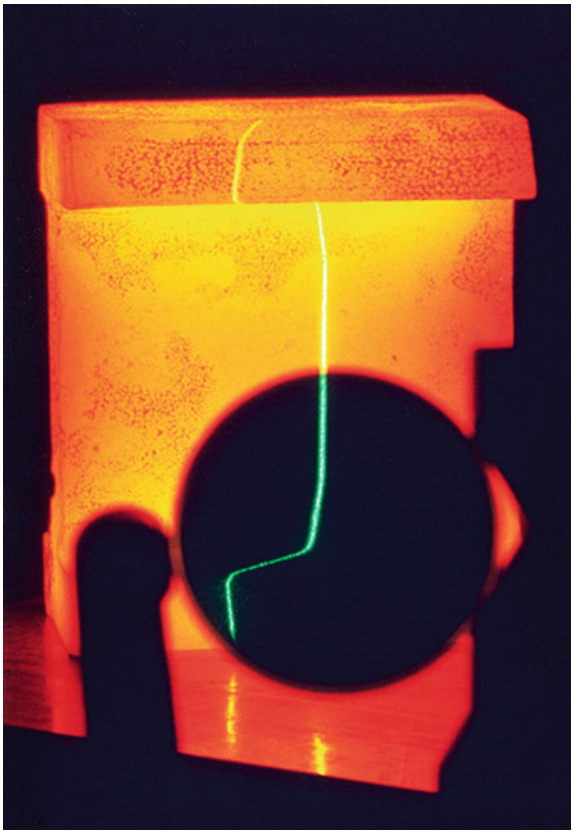

Fig. A.5 Photograph of a hot T-beam section illuminated by a laser light section. The dark black circle is a bandpass interference filter centered at the laser wavelength. The light passing the filter reveals a very high contrast which allows to follow the shape of the laser line even in the case of a strong luminous object

$$L_\lambda^{\text{laser}} = \frac{\phi}{\pi\left(\frac{d}{2}\right)^2 \Delta\Omega\Delta\lambda}. \tag{A.2.5}$$

Finally we obtain $L_\lambda^{\text{laser}} = 8.1 \times 10^7 \text{W}/(\text{cm}^2\text{sr nm})$, see data point shown as open triangle in Fig. A.4. This demonstrates that the spectral radiance of even a moderate laser with a flux of 1 mW only is by many orders of magnitude higher than the black body radiation calculated for temperatures up to 10,000 K.

Figure A.5 gives an experimental evidence of this significant difference in the spectral radiances. A laser light section, cf. Chap. 10, is projected onto a T-beam section. The scattered light is observed via a bandpass interference filter (black circular disk in Fig. A.5) with a width of about 10 nm centered at the laser wavelength. Behind this filter a very high contrast between the laser light and the black body radiation is observed which mirrors the above stated differences between the spectral radiances of a coherent and an incoherent light source. This unique feature is utilized to measure e.g. the flatness of hot heavy plates with laser triangulation, see Sect. 10.4, Figs. 10.24, 10.25 and 10.26.

A.3 Derivation of Equation (9.23)

We insert the spectrum of the light source (9.21) in (9.18) and integrate over the angular wave numbers to gain the quantity I, which we need to describe the signal for time-domain OCT, cf. (9.19):

$$I(z_\mathrm{r}) = \int_0^\infty \left(1 + \sum_{j=1}^{N} R_{\mathrm{m},j}\right) \frac{I_0}{\sqrt{\pi}\Delta k} \mathrm{e}^{-\left[\frac{k-k_0}{\Delta k}\right]^2} \mathrm{d}k + \cdots$$

$$\ldots + \int_0^\infty 2 \sum_{j=1}^{N} \sqrt{R_{\mathrm{m},j}} \frac{I_0}{\sqrt{\pi}\Delta k} \mathrm{e}^{-\left[\frac{k-k_0}{\Delta k}\right]^2} \cos\left(2k\left(z_\mathrm{r} - z_{\mathrm{m},j}\right)\right) \mathrm{d}k. \tag{A.3.1}$$

The autocorrelation term is neglected, cf. third term with double sum in (9.18). The first integral in (A.3.1) is easily evaluated by use of (9.22):

$$A = \left(1 + \sum_{j=1}^{N} R_{\mathrm{m},j}\right) I_0. \tag{A.3.2}$$

As abbreviation for the second integral to be solved we use:

$$B = \int_0^\infty \frac{I_0}{\sqrt{\pi}\Delta k} \mathrm{e}^{-\left[\frac{k-k_0}{\Delta k}\right]^2} \cos\left(2k\left(z_\mathrm{r} - z_{\mathrm{m},j}\right)\right) \mathrm{d}k. \tag{A.3.3}$$

With the substitution $k' = k - k_0$, and the abbreviation $\delta z_j = z_\mathrm{r} - z_{\mathrm{m},j}$ we obtain:

$$B = \int_{-k_0}^\infty \frac{I_0}{\sqrt{\pi}\Delta k} \mathrm{e}^{-\left[\frac{k'}{\Delta k}\right]^2} \cos\left((k' + k_0)2\delta z_j\right) \mathrm{d}k'. \tag{A.3.4}$$

Assuming $k_0 > 0$ and $k_0 \gg \Delta k$ the integrand of (A.3.4) has only significant positive values close to the origin of the k' axis. Since we assume that the width of this Gaussian function is small compared to k_0, we can approximate the integral of (A.3.4) by extending the lower integration limit from "$-k_0$" to minus infinity:

$$B \approx \int_{-\infty}^\infty \frac{I_0}{\sqrt{\pi}\Delta k} \mathrm{e}^{-\left[\frac{k'}{\Delta k}\right]^2} \cos\left((k' + k_0)2\delta z_j\right) \mathrm{d}k'. \tag{A.3.5}$$

With the trigonometric addition theorem $\cos(x + y) = \cos x \cos y - \sin x \sin y$, we have:

$$B \approx \frac{I_0}{\sqrt{\pi}\Delta k} \int_{-\infty}^\infty \mathrm{e}^{-\left[\frac{k'}{\Delta k}\right]^2} \left[\cos\left(k'2\delta z_j\right) \cos\left(k_0 2\delta z_j\right) - \sin\left(k'2\delta z_j\right) \sin\left(k_0 2\delta z_j\right)\right] \mathrm{d}k'. \tag{A.3.6}$$

The second summand is a point symmetric function with respect to k', whereas the Gaussian function is a symmetric function with respect to k' and the ordinate. Therefore, the integral of the product of the second summand and the Gaussian function becomes zero. So from (A.3.6) we come to:

$$B \approx \frac{I_0 \cos\left(k_0 2\delta z_j\right)}{\sqrt{\pi}\Delta k} \int_{-\infty}^{\infty} \mathrm{e}^{-\left[\frac{k'}{\Delta k}\right]^2} \cos\left(k' 2\delta z_j\right)\, \mathrm{d}k'. \tag{A.3.7}$$

From [1] the following definite integral is known:

$$\int_{-\infty}^{\infty} \mathrm{e}^{-a^2 x^2} \cos bx \;\mathrm{d}x = \frac{\sqrt{\pi}}{a} \mathrm{e}^{-\frac{b^2}{4a^2}}. \tag{A.3.8}$$

With $a = 1/\Delta k, b = 2\delta z_j$ and $x = k'$, we see that (A.3.8) is equivalent to (A.3.7) and finally get for (A.3.7):

$$B \approx \frac{I_0 \cos\left(k_0 2\delta z_j\right)}{\sqrt{\pi}\Delta k} \sqrt{\pi}\Delta k \mathrm{e}^{-\delta z_j^2 \Delta k^2} = I_0 \cos\left(k_0 2\delta z_j\right) \mathrm{e}^{-\delta z_j^2 \Delta k^2}. \tag{A.3.9}$$

Taking this result (A.3.9), we have now solved (A.3.1) and can write with resubstitution of the used abbreviations:

$$I(z_\mathrm{r}) = I_0 \left(1 + \sum_{j=1}^{N} R_{\mathrm{m},j}\right) + 2I_0 \sum_{j=1}^{N} \sqrt{R_{\mathrm{m},j}} \cos\left(2k_0\left(z_\mathrm{r} - z_{\mathrm{m},j}\right)\right) \mathrm{e}^{-\left(z_\mathrm{r} - z_{\mathrm{m},j}\right)^2 \Delta k^2}. \tag{A.3.10}$$

Relation (A.3.10) is identical to (9.23).

A.4 Derivation of Equation (9.26)

To solve the integral (9.26) we introduce a substitution $k' = k - k_0$:

$$\tilde{f} = \frac{\eta}{2\pi} \int_{-\infty}^{+\infty} \frac{I_0}{\sqrt{\pi}\Delta k} \mathrm{e}^{-\left[\frac{(k-k_0)}{\Delta k}\right]^2} \mathrm{e}^{\mathrm{i}kz} \mathrm{d}k = \frac{\eta I_0 \mathrm{e}^{\mathrm{i}k_0 z}}{2\pi\sqrt{\pi}\Delta k} \int_{-\infty}^{+\infty} \mathrm{e}^{-\left[\frac{k'}{\Delta k}\right]^2} \mathrm{e}^{\mathrm{i}k'z} \mathrm{d}k'. \tag{A.4.1}$$

Euler's formula says:

$$\mathrm{e}^{\mathrm{i}k'z} = \cos(k'z) + \mathrm{i}\, \sin(k'z). \tag{A.4.2}$$

With the help of (A.4.2) the definite integral in (A.4.1) can be decomposed as follows:

$$\int_{-\infty}^{+\infty} \mathrm{e}^{-\left[\frac{k'}{\Delta k}\right]^2} \mathrm{e}^{\mathrm{i}k'z} \mathrm{d}k' = \int_{-\infty}^{+\infty} \mathrm{e}^{-\left[\frac{k'}{\Delta k}\right]^2} \cos(k'z) \mathrm{d}k' + \mathrm{i} \int_{-\infty}^{+\infty} \mathrm{e}^{-\left[\frac{k'}{\Delta k}\right]^2} \sin(k'z) \mathrm{d}k'. \tag{A.4.3}$$

The first term on the right handside of (A.4.3) is a symmetric function of z (symmetric about the y-axis), whereas the second term is a point symmetric function with respect to z (symmetric about the origin). Hence, the second term on the right handside of (A.4.3) is zero. The first term is a known definite integral [1]:

$$\int_{-\infty}^{+\infty} \mathrm{e}^{-\left[\frac{k'}{\Delta k}\right]^2} \cos(k'z)\mathrm{d}k' = 2\int_{0}^{+\infty} \mathrm{e}^{-\left[\frac{k'}{\Delta k}\right]^2} \cos(k'z)\mathrm{d}k' = \sqrt{\pi}\Delta k \mathrm{e}^{-\frac{z^2\Delta k^2}{4}} \tag{A.4.4}$$

for $\Delta k > 0$. Inserting (A.4.4) in (A.4.1) then yields:

$$\tilde{f}(z) = \frac{\eta I_0 \mathrm{e}^{\mathrm{i}k_0 z}}{2\pi\sqrt{\pi}\Delta k}\sqrt{\pi}\Delta k \mathrm{e}^{-\frac{z^2\Delta k^2}{4}} = \frac{\eta I_0 \mathrm{e}^{\mathrm{i}k_0 z}}{2\pi}\mathrm{e}^{-\frac{z^2\Delta k^2}{4}} \tag{A4.5}$$

Relation (A.4.5) is identical to (9.26).

A.5 Derivation of Equation (9.27)

We start with (9.25), insert (9.20) and for I_k (9.18):

$$\tilde{S}(z) = \frac{\eta}{2\pi}\left\{\int_{-\infty}^{\infty} I_{0,k}\left(1 + \sum_{j=1}^{N} R_{\mathrm{m},j}\right)\mathrm{e}^{\mathrm{i}kz}\mathrm{d}k + \int_{-\infty}^{\infty} I_{0,k} 2 \sum_{j=1}^{N} \sqrt{R_{\mathrm{m},j}} \cos\big(k2\big(z_{\mathrm{r}} - z_{\mathrm{m},j}\big)\big)\mathrm{e}^{\mathrm{i}kz}\mathrm{d}k\right\}. \tag{A.5.1}$$

Relation (A.5.1) is decomposed in two summands. For the first summand we have with (9.21) and (9.26):

$$\tilde{S}_1(z) = \frac{\eta}{2\pi}\left(1 + \sum_{j=1}^{N} R_{\mathrm{m},j}\right) I_0 \mathrm{e}^{\mathrm{i}k_0 z}\mathrm{e}^{-\frac{z^2\Delta k^2}{4}} = \left(1 + \sum_{j=1}^{N} R_{\mathrm{m},j}\right)\tilde{f}(z). \tag{A.5.2}$$

For the second summand we obtain after insertion of (9.21) and the abbreviation $\Delta z_j = 2\big(z_{\mathrm{r}} - z_{\mathrm{m},j}\big)$:

$$\tilde{S}_2(z) = \frac{2\eta}{2\pi}\sum_{j=1}^{N}\sqrt{R_{\mathrm{m},j}}\frac{I_0}{\sqrt{\pi}\Delta k}\int_{-\infty}^{\infty} \mathrm{e}^{-\frac{(k-k_0)^2}{\Delta k^2}} \cos\big(k\Delta z_j\big)\,\mathrm{e}^{\mathrm{i}kz}\mathrm{d}k. \tag{A.5.3}$$

We abbreviate the definite integral with the letter B:

$$B = \int_{-\infty}^{\infty} \mathrm{e}^{-\frac{(k-k_0)^2}{\Delta k^2}} \cos\big(k\Delta z_j\big)\,\mathrm{e}^{\mathrm{i}kz}\mathrm{d}k. \tag{A.5.4}$$

With the substitution $k' = k - k_0$ follows from (A.5.4):

$$B = \int_{-\infty}^{\infty} \mathrm{e}^{-\frac{k'^2}{\Delta k^2}}\mathrm{e}^{\mathrm{i}k'z}\mathrm{e}^{\mathrm{i}k_0 z}\cos\big[(k' + k_0)\Delta z_j\big]\mathrm{d}k'. \tag{A.5.5}$$

With Euler's formula (A.4.2) this can be rewritten and decomposed in two summands:

$$B = \frac{\mathrm{e}^{\mathrm{i}k_0 z}}{2} \int_{-\infty}^{\infty} \mathrm{e}^{-\frac{k'^2}{\Delta k^2}} \mathrm{e}^{\mathrm{i}k' z} \left[\mathrm{e}^{\mathrm{i}(k'+k_0)\Delta z_j} + \mathrm{e}^{-\mathrm{i}(k'+k_0)\Delta z_j} \right] \mathrm{d}k', \tag{A.5.6}$$

$$B = \frac{\mathrm{e}^{\mathrm{i}k_0 z}}{2} (b_1 + b_2). \tag{A.5.7}$$

The summand b_1 can be converted as follows:

$$b_1 = \mathrm{e}^{\mathrm{i}k_0 \Delta z_j} \int_{-\infty}^{\infty} \mathrm{e}^{-\frac{k'^2}{\Delta k^2}} \mathrm{e}^{\mathrm{i}k' \left(z + \Delta z_j\right)} \mathrm{d}k'. \tag{A.5.8}$$

With Euler's formula (A.4.2) we see, that the integrand is again a sum of a symmetric and a point symmetric function, hence the integral over the second summand vanishes and we obtain:

$$b_1 = \mathrm{e}^{\mathrm{i}k_0 \Delta z_j} \int_{-\infty}^{\infty} \mathrm{e}^{-\frac{k'^2}{\Delta k^2}} \cos\left(k' \left(z + \Delta z_j\right)\right) \mathrm{d}k'. \tag{A.5.9}$$

This integral is known, cf. (A.3.8) and (A.4.4):

$$b_1 = \mathrm{e}^{\mathrm{i}k_0 \Delta z_j} \sqrt{\pi} \Delta k \mathrm{e}^{-\frac{\left(z + \Delta z_j\right)^2 \Delta k^2}{4}}. \tag{A.5.10}$$

Analogously we have for the second summand:

$$b_2 = \mathrm{e}^{-\mathrm{i}k_0 \Delta z_j} \sqrt{\pi} \Delta k \mathrm{e}^{-\frac{\left(z - \Delta z_j\right)^2 \Delta k^2}{4}}. \tag{A.5.11}$$

Now we insert these summands into relation (A.5.7):

$$B = \frac{\mathrm{e}^{\mathrm{i}k_0 z}}{2} \sqrt{\pi} \Delta k \left[\mathrm{e}^{\mathrm{i}k_0 \Delta z_j} \mathrm{e}^{-\frac{\left(z + \Delta z_j\right)^2 \Delta k^2}{4}} + \mathrm{e}^{-\mathrm{i}k_0 \Delta z_j} \mathrm{e}^{-\frac{\left(z - \Delta z_j\right)^2 \Delta k^2}{4}} \right]. \tag{A.5.12}$$

This can be rewritten with (A.4.5):

$$B = \frac{\sqrt{\pi} \Delta k}{2} \left[\frac{2\pi \tilde{f}\left(z + \Delta z_j\right)}{\eta I_0} + \frac{2\pi \tilde{f}\left(z - \Delta z_j\right)}{\eta I_0} \right]. \tag{A.5.13}$$

Going back to (A.5.3) and cancelling some terms we get:

$$\tilde{S}_2(z) = \sum_{j=1}^{N} \sqrt{R_{\mathrm{m},j}} \left(\tilde{f}\left(z + \Delta z_j\right) + \tilde{f}\left(z - \Delta z_j\right) \right). \tag{A.5.14}$$

Inserting (A.5.2) and (A.5.14) into (A.5.1) then finally yields:

$$\tilde{S}(z) = \tilde{f}(z)\left(1 + \sum_j R_{\mathrm{m},j}\right) + \left(\sum_j \sqrt{R_{\mathrm{m},j}}\left(\tilde{f}(z + \Delta z_j) + \tilde{f}(z - \Delta z_j)\right)\right). \quad \text{(A.5.15)}$$

The expression (A.5.15) is identical to (9.27).

References

1. I. Bronstein, K. Semendjajew, *Taschenbuch der Mathematik*, 19. Aufl. (Verlag Harri Deutsch, Thun Frankfurt, 1980), p. 118
2. A. Anders, *A Formulary for Plasma Physics* (Akademie-Verlag, Berlin, 1990)

Abbreviations

Abbreviation	Explanation	Chapter(s), Figure(s), Table(s)	Page numbers
A-, B-, C-scan	Depth scan, 2D scan, 3D scan	9.1, Fig. 9.2	228
ADC	Analog digital converter	14.6	382
BD	Blu-ray disc	12.3.1	315
BOXCARS	Variant of CARS, cf. Fig. 13.31	13.3.2	362
CD	Compact disc	12.3.1	314
DC term	Undiffracted reference wave	7.4.1	185
CARS	Coherent anti-Stokes Raman spectroscopy	13.3	355
CLSM	Confocal laser scanning microscope	12	305
CCD	Charge-coupled device	5.4.5, 10.2.4, Table 10.1, Fig. 5.38	135, 260, 261
CMOS	Complementary metal oxide semiconductor	10.2.4, Table 10.1	260, 261
CRM	Certified reference material	13.1.6	336
DON	Deoxynivalenol	14.7	388
DVD	Digital versatile disc	12.3.1	314
E-CARS	CARS in backward direction	13.3.4	368
ESPI	Electronic speckle interferometry	8.3.3, Fig. 8.11	213, 214
F-CARS	CARS in forward direction	13.3.4	367
FD-OCT	Fourier domain OCT	9.1.2, Fig. 9.19	235, 244
FLIM	Fluorescence lifetime imaging	14.6	382
FPS	Fluorescence polarization spectroscopy	14.5, Fig. 14.7	380, 381
FWHM	Full width at half maximum	12.1.2	307
IR	Infrared	5.4.3	131
LAM	Laser additive manufacturing	1	2
LDA	Laser Doppler anemometer	11.3, Fig. 11.3	292
LIDAR	Light detection and ranging	13.2, Fig. 13.17	343, 344
LIBS	Laser-induced breakdown spectroscopy	13.1, Fig. 13.1	324

(continued)

(continued)

Abbreviation	Explanation	Chapter(s), Figure(s), Table(s)	Page numbers
MEMS	Microelectromechanical systems	9.3	243
MESF	Molecules of equivalent soluble fluorophore	14.7	389
MOS	Metal-oxide-semiconductor	5.4.5, Fig. 5.37	134
MOSFET	Metal-oxide-semiconductor field effect transistor	5.4.5	134
NA	Numerical aperture	12.1.1, (12.1), 12.1.2, Table 12.1	306, 308, 315
OCT	Optical coherence tomography	9, Fig. 9.1	227
OPO	Optical parametric oscillator	13.3.1	360
PDA	Photodiode array	5.4.5	135
PET	Polyethylene terephthalate	9.3, Fig. 9.19	244
PIN	Positive-instrinsic-negative photodiode	5.3.2	121
PSF	Point-spread function	12.1.2	307
ROI	Region of interest	10.2.4	262
ptv	Peak-to-valley	7.5.2, Fig. 7.22	193
SEM	Scanning electron microscopy	12.3.1	315
TCSPC	Time correlated single photon counting	14.6, Fig. 14.8	382
TD-OCT	Time-domain optical coherence tomography	9.1.1, Fig. 9.3	229
UV	Ultraviolet	5.4.3, 9.3	131, 244
VCO	Voltage controlled oscillator	11.3.2, Fig. 11.16	296
VIS	Visible	5.4.3	131
2-D	Two dimensional	10.1, Fig. 10.2	249
3-D	Three dimensional	10.1, Fig. 10.2	249

Notations and list of symbols

The following notation rules are used in this book:

a) physical quantities are written with italic characters to visualize that these quantities have a unit, example: P, radiant flux; unit: Watt,
b) mathematical variables are also written with italic characters to clearly distinguish these from units or numbers, example: $j = 1, 2, \ldots$,
c) numbers including the imaginary unit $\mathrm{i} = \sqrt{-1}$, and the Euler number e are set with non-italic characters; mathematical functions are also set with non-italic characters, example J_0, zeroth order Bessel function,
d) units are set with non-italic characters to clearly distinguish these form the cases a), b); example: m, meter,
e) abbreviations for objects or denominations of points are set with non-italic characters, examples: r, stands for reference beam or P, denotes a point,
f) differentials are written with non-italic characters followed by a physical quantity written with italic character, example: dx.

Symbol	Description	Unit	Chapter(s), Figure(s), Formula(s)
a	Typical dimension of diffracting aperture	m	2.3, (2.16)
$A(\tau)$	Autocorrelation function	$[s(t)]^2$	11.3.2, (11.38)
A	Absorptance	1	5.1, (5.1), 13.1.3, (13.8),
A	Resolution	1	6.2.4
A_{ji}	Einstein coefficient for spontaneous emission for the transition from the upper level j to the lower level i	s^{-1}	13.1.3, (13.8)
α	Absorption coefficient	m^{-1}	3.3.1, (3.12), (7.7)
α	Angle of incident laser beam	rad	2.2.3, (2.10), 10.2.1, (10.9)
α	Temperature coefficient	1/K	5.1.2, (5.18)
α_x	Angle of deflection in the x-direction	rad	10.2.5, (10.35)
(α)	Specific rotation	rad/m	4.1.2, (4.6)
b	Image distance	m	8.2.1, (8.3)
b_λ	spectral intensity of the background radiation	W/m	13.1.5, (13.12)
B	Size of the image	m	8.2.1, (8.4), 10.1.1
B_ω	Angular spectrum bandwidth	rad s^{-1}	11.2.2, (11.18)
β	Opening angle of the objective	rad	10.2.4, (10.31)
$\beta(r,t)$	Scattering coefficient per solid angle per path length	$m^{-1}sr^{-1}$	13.2.1, (13.17)
c	Speed of light	m/s	2.1, 3.2, (2.4), (3.4)
c	Specific heat capacity	J/(kg K)	13.1.2, (13.3)
C_Q	Heat capacity	J/K	5.1, (5.1)
$\chi^{(1)}$	Electrical susceptibility of first order	As/(Vm)	13.3.1
d_{fp}	Displacement in the film plane	m	8.2.1, (8.5)
d_{op}	Displacement in the object plane	m	8.2.1, (8.6)
d_{Plasma}	Plasma diameter	M	13.1.4, (13.10)
d_{sp}	Speckle size	m	8.2.1, (8.7)
d_x	Object translation within the object surface	m	8.3.2, Table 8.1
d_z	Object translation perpendicular to the object surface	m	8.3.2, Table 8.1
$\vec{d}$	Displacement vector	m	8.3.2, (8.26), (8.28)
$d\Omega_{det}$	Solid angle of receiving optic	sr	13.2.1, (13.18)
D	Thickness of hologram, diameter of aperture	m	7.1, (7.7), 8.1, (8.2), Fig. 8.6, 10.2.4, (10.11)
D	Optical density	1	5.4.1, (5.55)
D_c	Diameter of circle enclosing the interference pattern in the observation plane	m	8.2.1, Fig. 8.4
D_{ph}	Pinhole diameter	m	12.1.2, (12.8)

(continued)

(continued)

Symbol	Description	Unit	Chapter(s), Figure(s), Formula(s)
δ_h	Heat penetration depth	m	13.1.1
δ_opt	Optical penetration depth	m	13.1.1
$\delta(z_\mathrm{m} - z_{\mathrm{m},j})$	Dirac function	m^{-1}	9.1.1, (9.11)
$\vartheta_{\mathrm{m,r}}(x, y)$	Phase of scattered waves in the observation plane	rad	8.3, (8.21)
Δ	Path difference	m	2.3.1, (2.19)
$\Delta\phi$	Phase difference	rad	8.2.2, (8.17)
$\Delta\Omega_\mathrm{c}$	Solid coherence angle	sr	2.4.3, (2.33)
ΔN_sp	Fluctuation of number of speckles per pixel	1	10.2.4
Δp	Width of pixel	m	10.2.4, Fig. 10.15
Δr_min	Lateral resolution	m	12.1.2, (12.5)
Δt	Temporal width	s	9.1.1, (9.1)
Δy	Height of pixel	m	10.2.4, Fig. 10.15
Δz	Uncertainty in the determination of the light spot on the z-axis	m	10.2.1, (10.9), Fig. 10.7, 10.2.4, (10.32)
$\Delta z'_\mathrm{cg}$	Measuring uncertainty in the determination of the position of the light spot in the detector plane	m	10.2.4, (10.25), (10.29)
e	elementary charge	C	5.1.3, (5.50)
$\vec{e}_\mathrm{i}$	Unit vector describing the direction of the incident wave	1	11.1
$\vec{e}_\mathrm{o}$	Unit vector describing the direction of the scattered wave	1	11.1
$\vec{E}$	Electric field strength vector	V/m	2.1, (2.1a)
$\vec{E}_0$	Electric field strength amplitude	V/m	2.1, (2.1a)
$E_{\mathrm{m},k}, E_{\mathrm{r},k}$	Complex spectral field strength in the measuring arm, reference arm	V/rad	9.1.1, (9.10)
E_o	Complex amplitude of the electric field of the object wave	V/m	7, (7.1)
E_o^d	Complex amplitude of the electric field of the object wave of the displaced object	V/m	Fig. 7.5, (7.8)
E_r	Complex amplitude of the electric field of the reference wave	V/m	7, (7.1), 9.1.1, (9.5)
ε	Slope of the linear part of an amplitude transmission curve	$\mathrm{m}^2/(\mathrm{Ws})$	7, (7.2)
ε_AB	Seebeck coefficient	V/K	5.1.1, (5.16)
ε_0	Permittivity of free space	$\mathrm{AsV}^{-1}\mathrm{m}^{-1}$	3.4.3, (3.20a)
$\varepsilon_{ji}^{\nu,\mathrm{d}\Omega}(t)$	Line emission coefficient of the transition $j \rightarrow i$	$\mathrm{W}/(\mathrm{m}^3\ \mathrm{sr}\ \mathrm{Hz})$	13.1.4, (13.9)
η	Modulation index	1	11.2.2, (11.7)

(continued)

(continued)

Symbol	Description	Unit	Chapter(s), Figure(s), Formula(s)
η	Quantum efficiency	1	5.3.1, (5.43)
F	Area	m^2	5.1.3, (5.25)
f, f_F	Focal length	m	7.1, Fig. 7.3, 8.2.1, (8.3), 10.1.1, (10.2), 10.2.1, (10.6)
f	Frequency	1/s	2.1, (2.4), 5.1.3, (5.50)
φ_0	Phase angle	rad	2.1 (2.1)
ϕ	Phase of the object wave	rad	7.1, (7.8)
ϕ_i	Phase shifts	rad	7.3.3, (7.19)
ϕ_{sp}	Size of speckles	m	10.2.4, (10.11)
g	Object distance	m	8.2.1, (8.3)
G	Size of the object	m	8.2.1, (8.4), 10.1.1
$\Gamma(\nu)$	Line profile as a function of the frequency	1/Hz	13.1.4, (13.9)
h	Planck constant	Js	3.1, 13.1.4, (13.9)
H	Brightness on the monitor	a.u.	8.3.3, (8.50)
H	Radiant exposure	J/m^2	5.4.1, (5.56)
$\vec{H}$	Magnetic field strength vector	A/m	2.1, (2.1b)
$\vec{H}_0$	Magnetic field strength amplitude	A/m	2.1, (2.1b)
i_{cg}	Center of gravity of the counter variable i	1	10.2.4, (10.12)
I	Intensity, irradiance	W/m^2	2.1, (2.6), 6.1.1, (6.5b)
I	Current	A	5.1.3, (5.29)
I_j	Intensity of an element line of an analyte j	a.u.	13.1.1
I_{ph}	Photovoltaic current	A	5.3.2, (5.50)
I_r	Intensity of a reference line	a.u.	13.1.1
$I(r)$	Intensity profile	W/m^2	10.2.2
$I(x, y)$	Irradiance as function of the coordinates x, y	W/m^2	7, (7.1)
$I'(z')$	Intensity distribution of the imaged light spot in the plane of detection	W/m^2	10.2.2
I_k	Spectral irradiance	W/(m rad)	9.1.1, (9.16a)
J_0	Zeroth order Bessel function	1	8.3.4, (8.57)
J_k	Line intensity of species k	a.u.	13.1.5, (13.13)
k	Angular wave number	rad m^{-1}	2.1, (2.3)
$\vec{k}_1, \vec{k}_2; \vec{k}, \vec{k}'$	Angular wave vectors of incident and scattered light	rad m^{-1}	7.1, (7.16), 8.3.2, (8.26)
K	Number of beam quality	1	2.6.3, (2.39)
K	Kerr's constant	m/V^2	3.2.4, (3.10)
κ	Constant	1	10.2.4, (10.29)
κ	Thermal diffusivity	m^2/s	13.1.2
$\vec{l}$	Displacement vector	m	7.1, (7.16)
L	Distance between mirrors	m	2.5, (2.34)

(continued)

(continued)

Symbol	Description	Unit	Chapter(s), Figure(s), Formula(s)
L	Distance between scattering surface and observation screen	m	2.3, (2.16), 8.1, (8.1)
L_c	Coherence length	m	2.4 (2.28), 9.1.1, (9.1)
λ	Wavelength	m	2.1, (2.3), 8.1, (8.1)
Λ	Wavelength	m	4.1.1, (4.4)
m_L	Slope	1	10.1.1, (10.1), Fig. 10.4
M_φ	Angle enlargement	1	7.1
M_z	Enlargement in the z-direction	1	7.1
M_z	Measuring range in z-direction	m	10.2.1, (10.8)
M	Ray transfer matrix	N/A	4.2.1, (4.22)
M	Number of modes	1	4.3.1, (4.64)
M^2	Beam propagation ratio	1	2.6.3, (2.42)
$\mu(\lambda, R)$	Spatial dependent extinction coefficient	m^{-1}	13.2.1, (13.15)
n	Integer	1	7.1, (7.11)
n	Refractive index	1	3.2.2, 7.1, (7.7), 10.2.5, (10.35)
N	Resolving power	1	10.2.1, (10.10)
NA	Numerical aperture	1	12.1.2, (12.4)
N_a^z	Density of species a with charge z	m^{-3}	13.1.4, (13.9)
N_{sp}	Number of speckles per pixel	1	10.2.4
ν_{ji}	Frequency of the transition from $j \rightarrow i$	Hz	13.1.4, (13.9)
ω	Angular frequency of oscillation	rad s^{-1}	2.1, (2.1), 8.3.4, (8.53)
p	Momentum	kg m s^{-1}	3.1, (3.2)
p	Pyroelectric coefficient	C m^{-2} K^{-1}	5.1.3, (5.28)
$\vec{P}$	Electrical polarization	As/(m^2)	3.5, (3.20a), 13.3.1, (13.32)
P	Power	W	5.1, (5.1)
P	Radiant flux	W	5.3.2, (5.50)
q	Natural number	1	2.5, (2.34)
q	Complex beam Parameter	m	4.2.1, (4.18)
Q	Charge	C	5.2.1, (5.36)
Q_i	Radiant energy received by pixel element i	J	10.2.4, (10.12)
r	Electro-optical coefficient	m/V	3.2.4, (3.11)
r_m	Reflection coefficient of the measuring object	1	9.1.1, (9.6)
R	Distance between light source and diffracting aperture	m	2.3, (2.16)
R	Reflectivity, reflectance	1	3.2.2, (3.6), 4.1.1, (4.2) 13.1.2, (13.4)
R	Resistance	Ω	5.1.2, (5.18)

(continued)

(continued)

Symbol	Description	Unit	Chapter(s), Figure(s), Formula(s)
$R_{m,j}$	Reflectivity in the measurement path at location j	1	9.1.1, (9.17)
R_Q	Thermal resistance	K/(Wm^2)	5.1, (5.2a)
r_b	Beam radius	m	13.1.2, (13.2)
$r_{m,z_m}(z_m)$	Reflection coefficient in the measurement path per unit length	m^{-1}	9.1.1, (9.11)
ρ	Radius of curvature of the phase surfaces	m	2.6, (2.40)
ρ	Density	kg/m^3	13.1.2, (13.3)
$s(t)$	Local enlongation	m	8.3.4, (8.53)
s_{cg}	Standard deviation of i_{cg}	1	10.2.4, (10.19)
s_i	Distance between objective and image plane	m	10.2.4, (10.11)
s_{opt}	Optical path length	m	4.1.4, (4.15)
S	Spin	Js	3.1, (3.3)
S_k	Signal of Fourier-domain OCT depending on the angular wavenumber at constant position of the reference mirror	a.u.	9.1.1, (9.20), 9.1.2
S_λ	Spectral intensity	W/m	13.1.5, (13.11)
$S(z_r)$	Signal of time-domain OCT as a function of the position of the reference mirror	a.u.	9.1.1, (9.19)
$\tilde{S}(z)$	Inverse Fourier transform of S_k	a.u.	9.1.2, (9.25), (9.27)
$\vec{S}$	Poynting vector	W/m^2	6.1.1
$\sigma_i(\lambda)$	Absorption cross-section of the gas i at the wavelength λ	m^2	13.2.1, (13.28)
Σ	Sensitivity	K/W	5.1, (5.7)
t	Complex amplitude transmission	1	(7.7)
t	Time	s	
T	Transmittance	1	3.3.2, (3.15)
T	Integration time of the video camera	s	8.3.4, (8.56)
T	Temperature	K	5.1, (5.1), 13.1.2, (13.3)
T_0	Transmittance at low intensities	1	3.3.2, (3.15)
T_b	Beat period	s	2.2, (2.13), 11.2.1, (11.12)
T_c	Coherence time	s	2.4.1, (2.28), 9.1.1, (9.2a)
τ	Exposure time	s	5.4.1, (5.56), 7, (7.2)
τ_D	Time constant of the detector	s	13.2.1, (13.21)
τ_L	Duration of the laser pulse	s	13.2.1, (13.21)
θ_0	Opening angle of Gaussian beam	rad	2.6.1, (2.39)
θ_B	Brewster angle	rad	3.2.2, (3.7)
θ_t	Critical angle of total reflection	rad	3.2.2, (3.8)

(continued)

(continued)

Symbol	Description	Unit	Chapter(s), Figure(s), Formula(s)
u, v	Coordinates	m	10.1.1, (10.1)
$u_a^z(T)$	Partition function of species a with charge z	1	(13.1.4), (13.9)
U	Voltage of video signal	V	8.3.3, (8.48)
$U_{\lambda/2}$	Half-wave voltage	V	4.1.3, (4.10)
v_R	Velocity of the reference mirror	m/s	9.1.1, (9.1)
v_{th}	Average thermal speed of the atoms and ions in the plasma	m/s	13.1.4, (13.10)
$\vec{v}$	Velocity vector	m/s	11.1, (11.5)
V	Verdets's constant	rad/A	4.1.2, (4.7)
w, w_0	Waist radius of laser beam	m	2.6.1, (2.37a), 4.2.1, (4.19), 10.2.1
W	Photon energy	J	3.1, (3.1)
W_W	Work function	J	5.1.3, (5.33)
z_m	Position of measuring object	M	9.1.1, (9.6)
z_r	Position of reference mirror	m	9.1.1, (9.5)

(continued)

Index

A. Donges and R. Noll, *Laser Measurement Technology*, Springer Series in Optical Sciences 188, DOI: 10.1007/978-3-662-43634-9,